

# Estimation of light interception properties of conifer shoots by an improved photographic method and a 3D model of shoot structure

MATHIEU THÉRÉZIEN,<sup>1,2</sup> SARI PALMROTH,<sup>1</sup> RACHAEL BRADY<sup>3</sup> and RAM OREN<sup>1</sup>

<sup>1</sup> Nicholas School of Environmental & Earth Sciences, Duke University, Durham, NC 27708-0328, USA

<sup>2</sup> Corresponding author (mathieu.therezien@duke.edu)

<sup>3</sup> Visualization Technology Group, Duke University, Durham, NC 27708-0328, USA

Received November 26, 2006; accepted February 16, 2007; published online July 3, 2007

**Summary** The spherical mean of the shoot silhouette-to-total leaf area ratio ( $\overline{\text{STAR}}$ ) and the shoot transmission coefficient ( $c$ ) are two key structural parameters in radiative transfer models for calculating canopy photosynthesis and leaf area index. The standard optical method for estimating these parameters might introduce errors in the estimates for species with flexible shoots and needles by changing shoot inclination relative to its inclination in situ. We devised and tested two methods to address this problem. First, we modified the standard optical method by designing an apparatus that allows shoots to be photographed in their original orientation. Second, we developed a faster, model-based approach to replace photography and tested the results against the established approach. We used shoots of three pine species, *Pinus echinata* Mill. (needle length ~50 mm), *P. taeda* L. (~150 mm) and *P. palustris* Mill. (~300 mm). Values of the parameters simulated by the model were similar to those measured from the photographs. In our data,  $\overline{\text{STAR}}$  varied about twofold among the pine species and was ~40% higher in shade shoots than in sun shoots of *P. taeda*. The transmission coefficient for *P. taeda* shade shoots was also ~40% higher than that of sun shoots of all three species. We tested the versatility of the model by employing it on shoots of two other pine species (*P. strobus* L. and *P. thumbergiana* Parl.) as well as on shoots of *Tsuga canadensis* L. Carr. and *Picea pungens* Engelm. Regardless of shoot characteristics, the model generated values of shoot structural parameters similar to those estimated with the optical method. Although species-specific and vertical gradients in parameter values are best for modeling radiative transfer in conifer canopies, our results suggest that, in the absence of adequate data,  $\overline{\text{STAR}}$  can be approximated as 0.16 for a wide range of shoot structures. For applications requiring angle-dependent parameterization, our new model facilitates rapid generation of these radiative transfer parameters.

**Keywords:** L-systems, needle area, *Pinus echinata*, *Pinus palustris*, *Pinus taeda*, shoot silhouette-to-leaf area ratio, transmission coefficient.

## Introduction

Leaf-level photosynthetic responses are scaled to canopies based on the amount of photosynthetically active radiation (PAR) incident on the leaf surfaces. Because the PAR regime on leaf surfaces cannot be routinely measured, it must be simulated with radiative transfer models (RTMs). The RTMs describe the interaction between incoming solar radiation and the amount and distribution of canopy elements. The same principles can also be used to invert optically measured canopy transmittance or reflectance and estimate leaf area index (LAI; e.g., Miller 1967, Anderson 1971, Ross 1981, Nilson and Ross 1997, Knyazikhin et al. 1998). In most cases, estimation of canopy photosynthesis, typically the largest CO<sub>2</sub> flux in forest ecosystems, relies on both indirect estimates of LAI and modeled distributions of PAR on leaf surfaces and, therefore, on the ability of models to simulate realistic canopies.

In conifers, the arrangement of shoot needles adds structure to the canopy architecture with implications for the radiation regime. At a given LAI, clumping of needles into shoots causes self-shading within the shoot but increases the depth to which radiation penetrates the canopy (Norman and Jarvis 1975, Oker-Blom and Smolander 1988, Nilson and Ross 1997). Clumping of needles into shoots also affects canopy reflective properties by increasing the probability of multiple scattering within a shoot, thus decreasing reflectance (Knyazikhin et al. 1998, Shabanov et al. 2000, Smolander and Stenberg 2003, 2005). In canopy PAR interception and photosynthesis models, shoot structure can be incorporated by replacing the mean projection of unit flat area ( $G$ ; Nilson 1971) by the mean ratio of shoot silhouette area to total needle area ( $\overline{\text{STAR}}$ ; Oker-Blom and Smolander 1988). Furthermore,  $\overline{\text{STAR}}$  is related to the shoot clumping factor, or shading factor ( $\beta = 4\overline{\text{STAR}}$ ; Stenberg et al. 1994), which can be used to correct estimates of LAI obtained from ground-based transmittance measurements (Stenberg 1996, Chen et al. 1997). Recently, Smolander and Stenberg (2003, 2005) proposed a wavelength-dependent correction for the scattering coefficient in reflectance models, and showed how the probability of interaction within a shoot is closely related to  $\overline{\text{STAR}}$ . Although

STAR is fundamental to characterizing radiation regimes in coniferous canopies, it is rarely estimated accurately for each application.

In canopy photosynthesis models, shoot and needle structures are related to the phenomenon of partial shading, or penumbra (Miller and Norman 1971). The amount of penumbral PAR depends on the depth of the canopy, the distribution of the shoots and their “transparency,” i.e., the dimensions of the needles and their organization in shoots. Stenberg (1998) quantified this transparency with a transmission coefficient ( $c$ ), the mean gap area within the projected shoot envelope area. Thus defined, shading of one shoot by another reduces the fraction of visible sun by a factor of  $c$ . As a result, penumbra leads to a more even distribution of PAR on needle surfaces at a given canopy depth without affecting the mean PAR. Despite the potentially significant effects on canopy photosynthesis, penumbra is seldom taken into account in models (but see Wang et al. 1991, Stenberg 1998, Ryel et al. 2001, Schäfer et al. 2003).

There are few published values of  $\overline{STAR}$  for conifers (Table 1) and even fewer of  $c$  (Stenberg 1998; see Table 1). The considerable variability apparent in the shoot structure of coniferous species is reflected in the variation in these parameter values (Table 1). This means that  $\overline{STAR}$  and  $c$  for one species should not be used in the canopy RTM of another species. Furthermore, shoot structure varies greatly within the canopy because of shading (Sprugal et al. 1996, Stenberg et al. 1999, 2001, Palmroth et al. 2002, Cescatti and Zorer 2003), meaning that structural parameters obtained from one light environment should not be employed throughout the canopy. Thus, for each species, potentially large sampling is needed to characterize the vertical pattern in structural parameters.

Currently, shoot silhouette area is measured optically: the shoot is rotated in front of a fixed camera; a picture is taken from each angle; the shoot silhouette area is extracted from each picture (e.g., Palmroth et al. 2002); and the spherical mean is calculated. Although time consuming, this method is useful for shoots with short and stiff needles and stiff twigs that maintain the same three-dimensional structure regardless of the orientation of the shoot. However, orientation affects both twig and needle bending in long shoots with long, flexible needles, such as those of many pines, making the standard photographic method prone to error. Nevertheless, this method was recently used to analyze the characteristics of pine shoots with flexible elements (Niinemets et al. 2006). The technical difficulties of obtaining such data for flexible shoots and the time needed to obtain representative estimates of shoot parameters by the current optical approach contribute to the oversimplified parameterization of coniferous forests in RTMs.

We present two methods to estimate  $\overline{STAR}$  and  $c$  for shoots of any structure. First, we modified the existing photographic method to accommodate large shoots having flexible elements. Second, we developed a new 3D model that generates virtual representations of shoots based on a few readily obtained measurements. Using both methods, we estimated  $\overline{STAR}$  and  $c$  on shoots of three major southern pine species: *Pinus echinata* Mill. (shortleaf pine), *P. taeda* L. (loblolly pine, both sun and shade shoots) and *P. palustris* Mill. (long-

leaf pine). The shoot structure of these species differs considerably because of large variations in needle length (*P. echinata* ~50 mm; *P. taeda* ~150 mm; and *P. palustris* ~300 mm) and flexibility. Further, we tested the generality of the model by employing it on shoots of four species having shoots with different characteristics from those of the three intensively studied species: *Pinus strobus* L. (eastern white pine), *Pinus thunbergiana* Parl. (Japanese black pine), *Tsuga canadensis* L. Carr. (eastern hemlock) and *Picea pungens* Engelm. (Colorado blue spruce). The chosen species not only challenge the model, but add data on shoot structure to the published literature.

## Materials and methods

The primary variables estimated with both approaches were the shoot silhouette area ( $SSA(\phi, \theta)$ ), where  $\phi$  and  $\theta$  are the azimuth and zenith angles, respectively; Figure 1), shoot envelope area ( $SEA(\phi, \theta)$ ), defined as the outline of the convex hull of shoots, total needle area ( $A_N$ ) and total twig area ( $A_T$ ). Using the estimates of  $SSA(\phi, \theta)$ ,  $SEA(\phi, \theta)$ ,  $A_N$ , and  $A_T$ ,  $\overline{STAR}$  was calculated as (adapted from Stenberg et al. 1999):

$$\begin{aligned}\overline{STAR} &= \frac{1}{2\pi(A_N + A_T)} \int_{-\frac{\pi}{2}}^{\frac{\pi}{2}} \int_{-\frac{\pi}{2}}^{\frac{\pi}{2}} SSA(\phi, \theta) \cos(\theta) d\theta d\phi \\ &= \frac{1}{2\pi} \int_{-\frac{\pi}{2}}^{\frac{\pi}{2}} \int_{-\frac{\pi}{2}}^{\frac{\pi}{2}} STAR(\phi, \theta) \cos(\theta) d\theta d\phi\end{aligned}\quad (1)$$

We employed a similar formulation to calculate  $c$ :

$$c = \frac{1}{2\pi} \int_{-\frac{\pi}{2}}^{\frac{\pi}{2}} \int_{-\frac{\pi}{2}}^{\frac{\pi}{2}} \frac{SEA(\phi, \theta) - SSA(\phi, \theta)}{SEA(\phi, \theta)} \cos(\theta) d\theta d\phi\quad (2)$$

## Sampling

*Pinus taeda* shoots were collected from forest trees growing in a stand with a mean height of 17 m. The canopy is closed and the peak LAI (based on projected leaf area) is 5.6 (McCarthy et al. 2007). We sampled 10 shoots from the uppermost whorl and 10 shoots from the lowest living whorl of *P. taeda* trees accessible from towers. In other locations within the same region, nine *P. echinata* and eight *P. palustris* shoots were sampled from branches acclimated to high light in the outermost lower crown of isolated trees. Finally, we sampled a single shoot from light-acclimated branches of each of four additional species at the Sarah P. Duke Gardens of Duke University: *P. strobus*, *P. thumbergiana*, *Tsuga canadensis* and *Picea pungens*. Shoots collected early in the study (four from *P. echinata*, five each from sun and shade branches of *P. taeda* and one of *P. palustris*) were subjected to fewer measurements than those processed later (see Table 2); these shoots were omitted from the validation of the 3D shoot model.

We collected first-flush shoots formed during the previous year with as few dry needles as possible. In addition, two of the

Table 1. Comparison of results of studies of silhouette-to-leaf area ratios (STAR) and transmission coefficient ( $c$ ) of coniferous species. Measurements of STAR<sub>max</sub> were made at the particular incidence angle that maximizes the spherical mean of STAR (STAR) for each shoot. STAR does not account for twig correction. Corrected STAR adds total twig area to total needle area and modeled STAR removes twig from the modeled shoot. Means are averaged among sampled shoots and do not represent canopy means. Values in parentheses are standard deviations, if available, or minimum and maximum observed values (decrease observed with increasing openness). Abbreviations: C, control; and IL, irrigated and fertilized.

Species	STAR <sub>max</sub>	STAR	Corrected STAR	Modeled STAR <sup>1</sup>	$c$	Source
<i>Abies alba</i>	0.18 (0.1–0.3) <sup>2</sup>	0.11 (0.07–0.17) <sup>2</sup>	–	–	–	Cescatti and Zorer 2003
<i>Abies amabilis</i>	0.28 (0.11)	–	–	–	–	Leverenz and Hinckley 1990
<i>Abies amabilis</i>	0.221 (0.037) <sup>3</sup>	–	–	–	–	Sprugel et al. 1996
<i>Abies amabilis</i>	0.177 (0.107–0.316) <sup>3</sup>	0.114 (0.083–0.179) <sup>3</sup>	–	–	–	Stenberg et al. 1998
<i>Abies grandis</i>	0.32 (0.044)	–	–	–	–	Leverenz and Hinckley 1990
<i>Abies lasiocarpa</i> (sun)	0.15	–	–	–	–	Carter and Smith 1985
<i>Abies lasiocarpa</i> (shade)	0.31	–	–	–	–	Carter and Smith 1985
<i>Abies lasiocarpa</i>	0.21 (0.087)	–	–	–	–	Leverenz and Hinckley 1990
<i>Abies procera</i>	0.23 (0.071)	–	–	–	–	Leverenz and Hinckley 1990
<i>Casuarina glauca</i>	–	0.182 (0.143–0.249) <sup>5</sup>	–	–	–	Ninemets et al. 2006
<i>Picea abies</i>	0.27 (0.11)	–	–	–	–	Leverenz and Hinckley 1990
<i>Picea abies</i> (C)	0.210 (0.030) <sup>3</sup>	0.161 (0.020) <sup>3</sup>	–	–	–	Stenberg et al. 1995
<i>Picea abies</i> (IL)	0.289 (0.059) <sup>3</sup>	0.216 (0.042) <sup>3</sup>	–	–	–	Stenberg et al. 1995
<i>Picea abies</i> (C)	0.186 (0.031)	0.129 (0.017)	–	–	–	Palmroth et al. 2002
<i>Picea abies</i> (IL)	0.237 (0.039)	0.151 (0.018)	–	–	–	Palmroth et al. 2002
<i>Picea engelmannii</i> (sun)	0.12	–	–	–	–	Carter and Smith 1985
<i>Picea engelmannii</i> (shade)	0.18	–	–	–	–	Carter and Smith 1985
<i>Picea mariana</i>	–	0.126 (0.118–0.135) <sup>4</sup>	–	–	–	Chen et al. 1997
<i>Picea orientalis</i>	0.26 (0.087)	–	–	–	–	Leverenz and Hinckley 1990
<i>Picea sitchensis</i>	0.24 (0.087)	–	–	–	–	Leverenz and Hinckley 1990
<i>Pinus banksiana</i> (young)	–	0.152 (0.118–0.195) <sup>4</sup>	–	–	–	Chen et al. 1997
<i>Pinus banksiana</i> (old)	–	0.140 (0.118–0.178) <sup>4</sup>	–	–	–	Chen et al. 1997
<i>Pinus contorta</i> (sun)	0.13	–	–	–	–	Carter and Smith 1985
<i>Pinus contorta</i> (shade)	0.14	–	–	–	–	Carter and Smith 1985
<i>Pinus contorta</i>	0.16 (0.11)	–	–	–	–	Leverenz and Hinckley 1990
<i>Pinus contorta</i>	–	0.116 (0.067–0.20)	–	–	–	Oker-Blom et al. 1991
<i>Pinus echinata</i>	0.212 (0.067)	0.186 (0.053)	0.172 (0.039)	0.191 (0.038)	0.576 (0.097)	This study
<i>Pinus palustris</i>	–	0.161 (0.128–0.186) <sup>5</sup>	–	–	–	Ninemets et al. 2006
<i>Pinus palustris</i>	0.193 (0.053)	0.160 (0.037)	0.158 (0.036)	0.170 (0.016)	0.586 (0.105)	This study
<i>Pinus patula</i>	–	(0.098–0.186) <sup>5</sup>	–	–	–	Ninemets et al. 2006
<i>Pinus radiata</i>	–	0.091 (0.068–0.133) <sup>5</sup>	–	–	–	Ninemets et al. 2006
<i>Pinus sylvestris</i>	0.17 (0.055)	–	–	–	–	Ninemets et al. 2006
<i>Pinus sylvestris</i>	(0.103–0.249)	0.142 (0.022)	–	–	–	Leverenz and Hinckley 1990
<i>Pinus sylvestris</i>	0.170	0.147 (0.043)	–	–	–	Oker-Blom and Smolander 1988
<i>Pinus sylvestris</i>	–	–	–	–	0.4	Smolander et al. 1994
<i>Pinus sylvestris</i>	0.170 (0.030)	–	–	–	–	Stenberg 1998
<i>Pinus taeda</i> (sun)	0.178 (0.043)	0.161 (0.033)	0.153 (0.032)	–	–	Stenberg et al. 2001
<i>Pinus taeda</i> (shade)	0.263 (0.062)	0.152 (0.029)	0.149 (0.028)	0.155 (0.011)	0.609 (0.095)	This study
<i>Pseudotsuga menziesii</i>	0.28 (0.087)	0.222 (0.040)	0.218 (0.040)	0.192 (0.010)	0.850 (0.041)	This study
<i>Tsuga heterophylla</i>	0.27 (0.022)	–	–	–	–	Leverenz and Hinckley 1990
						Leverenz and Hinckley 1990

Continued on overleaf

Table 1 Cont'd. Comparison of results of silhouette-to-leaf area ratios (STAR) and transmission coefficient ( $c$ ) of coniferous species. Measurements of  $STAR_{max}$  were made at the particular incidence angle that maximizes the spherical mean of STAR (STAR) for each shoot. STAR does not account for twig correction. Corrected STAR adds total twig area and modeled STAR removes twig from the modeled shoot. Means are averaged among sampled shoots and do not represent canopy means. Values in parentheses are standard deviations, if available, or minimum and maximum observed values (decrease observed with increasing openness).

Species	$STAR_{max}$	STAR	Corrected STAR	Modeled STAR <sup>1</sup>	$c$	Source
<i>Picea pungens</i> <sup>6</sup>	0.192	0.176	0.166	—	0.365	This study
<i>Pinus palustris</i> (curr. year)	0.127	0.111	0.110	—	0.514	This study
<i>Pinus strobus</i> <sup>6</sup>	0.202	0.185	0.184	—	0.684	This study
<i>Pinus thumbergiana</i> <sup>6</sup>	0.201	0.198	0.192	—	0.708	This study
<i>Tsuga canadensis</i> <sup>6</sup>	0.398	0.265 <sup>7</sup>	0.239 <sup>7</sup>	—	0.426	This study

<sup>1</sup> Modeled averages and standard deviations computed from fewer samples than measured ones (see Table 2).

<sup>2</sup> Computed from the slope and intercept in Cescatti and Zorer (2003).

<sup>3</sup> Estimated with  $SPAR = \pi STAR$ , where SPAR is the silhouette to projected area ratio.

<sup>4</sup> Calculated from  $STAR = 0.5G\Omega$  with  $G$  the extinction coefficient function (Nilson 1971) estimated from plots in Niinemets et al. (2006) and  $\Omega$  the clumping index (Chen et al. 1997).

<sup>5</sup> Calculated from  $STAR = 0.25\Omega$ .

<sup>6</sup> These estimates were computed for one or two (current year of *P. palustris*) shoots only.

<sup>7</sup> For *T. canadensis*, total needle area included the one sided area of the very short needles covering the upper side of the twig.

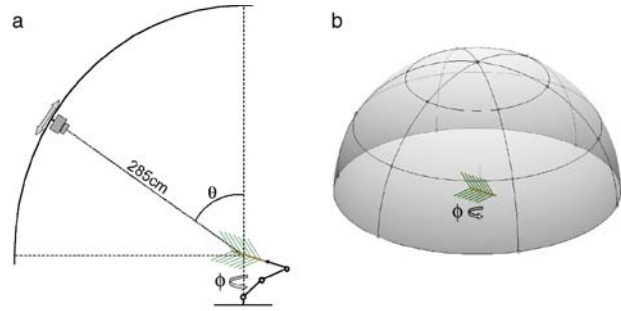


Figure 1. Schematic representation of the experimental apparatus.

eight *P. palustris* sample shoots were current-year shoots. The orientation of each shoot was measured with a compass (absolute  $\phi$ ) and a protractor (absolute  $\theta$ ) at the base of the shoot. The shoot was then cut from the branch and brought to the laboratory with the cut end set in water and the shoot protected so the structure was not altered.

#### Modified optical approach

**Measurements** In the laboratory, each shoot was first photographed with a camera (Nikon E8700 digital camera, Japan) attached to a fixed arcing arm (285-cm radius; Figure 1a). The camera was positioned at defined zenith angles, pointing to a shoot located at the center of the arc. This setup ensured a distance between the shoot and the camera that is large relative to the shoot dimensions, allowing angle distortions due to non-orthographic view to be ignored. The shoot was set at the same angular position as on the tree and then attached to an articulated arm fixed on a rotating base so that the shoot's geometrical center was directly above the rotation axis of the base. This setup eliminated the need to change the camera distance from the shoot when rotating the arm. The bottom of the shoot was delineated by black tape around the twig just below the first needle.

Purple fleece material was used as background behind the shoot. This background was chosen because it was non-reflective, did not interfere with the shoot colors and was easily removed from the photographs. Nineteen pictures ( $3264 \times 2448$  pixels), with a native 8.9–71.2 mm lens (35 mm format equivalent to 35–280 mm), were taken of each shoot. Pictures were taken at six azimuth angles ( $\phi = 0, 60, 120, 180, 240$  and  $300^\circ$ ) at each of the three zenith angles ( $\theta = 90, 60$  and  $30^\circ$ ), and one additional picture at  $\theta = 0^\circ$  (Figures 1a and 1b). Each time the position of the camera changed, a reference sphere with a known dimension was put next to the shoot in the field of view.

After the photographs were taken, twig length, twig diameter and  $\theta$  at the base and at the tip of the shoot were measured. Fascicles were counted. We measured the needle dimensions of 25 to 60 fascicles per shoot. This corresponded to about 20% of the fascicles on large shoots of *P. palustris* and up to 100% of the fascicles on small shoots of *P. echinata* and *P. taeda*. In the case of large shoots, the measured fascicles were chosen at even intervals spirally around the twig. Before dislodging the fascicle, the angle between the axis of each fas-

Table 2. Ranges of input and calculated variables for the three intensively studied species. Both sun and shade shoots of *Pinus taeda* were sampled, whereas only sun shoots of the other species were sampled. Values in parenthesis represent 1 SD. Abbreviations:  $N$ , number of sampled shoots;  $A_N$ , total needle surface area; SSA, spherical mean of the shoot silhouette area; STAR, spherical mean of the shoot silhouette-to-total leaf area ratio; and  $c$ , spherical mean of the shoot transmission coefficient.

	Unit	<i>Pinus echinata</i>	<i>Pinus taeda</i> (shade)	<i>Pinus taeda</i> (sun)	<i>Pinus palustris</i>
<i>Input variables</i>					
$N^1$	–	5	5	5	5
Fascicles	–	64.0 (24.7)	44.2 (13.6)	91.0 (32.3)	142 (12.6)
<i>Needle</i>					
Length	mm	40.1 (4.04)	148 (39.5)	140 (8.94)	290 (26.4)
Angle /twig	°	53.5 (4.66)	71.3 (10.2)	40.9 (2.76)	65.7 (5.57)
Width	mm	1.15 (0.022)	1.33 (0.072)	1.39 (0.095)	1.58 (0.141)
Density	mm <sup>-1</sup>	1.95 (1.35)	1.62 (0.407)	1.16 (0.227)	2.13 (0.496)
Deflection	m m <sup>-1</sup>	0.096 (0.013)	0.150 (0.049)	0.096 (0.019)	0.391 (0.120)
<i>Twig</i>					
Length	mm	93.8 (52.7)	59.1 (27.6)	159 (52.1)	137 (25.7)
Diameter	mm	2.95 (0.518)	5.07 (1.32)	7.12 (1.10)	16.6 (2.82)
Initial angle	°	48.9 (11.5)	43.4 (29.3)	36.4 (16.9)	49.4 (18.3)
Final angle	°	44.3 (5.70)	49.4 (41.1)	26.6 (22.3)	42.8 (21.5)
<i>Calculated variables</i>					
$N^1$	–	9	10	10	8
$A_N$	10 <sup>3</sup> mm <sup>2</sup>	17.4 (6.68)	61.5 (32.5)	171 (88.0)	659 (295.8)
SSA	10 <sup>3</sup> mm <sup>2</sup>	3.03 (0.897)	13.0 (6.04)	26.4 (14.5)	97 (21.8)
STAR	–	0.172 (0.039) <sup>2</sup>	0.218 (0.040) <sup>3</sup>	0.148 (0.028) <sup>2,3</sup>	0.170 (0.016) <sup>2</sup>
$c$	–	0.576 (0.097) <sup>2</sup>	0.850 (0.041) <sup>3</sup>	0.609 (0.095) <sup>2,3</sup>	0.633 (0.093) <sup>2</sup>

<sup>1</sup> Shoots measured early in the study were not used for model validation.

<sup>2</sup> Sample means of STAR and  $c$  in sun shoots did not differ significantly among species (one-way ANOVA;  $P = 0.189$ ).

<sup>3</sup> Sample means of STAR and  $c$  differed significantly between sun and shade shoots of *P. taeda* (Student  $t$ -test;  $P < 0.001$ ).

cicle and the main twig axis was measured with a specially designed compass. Needle length was then determined with a caliper or ruler, and needle width with a graduated lens. Next, to obtain an estimate of projected needle area ( $A_{PN}$ ), all needles of each shoot were laid flat without overlap on neutral color, non-reflective fabric, and a picture was taken of the needles together with the reference sphere. We replaced this last step by a model-based estimate of leaf area (described later) after we found no significant difference between estimates obtained with the two methods.

**Image analysis** For each image, the diameter of the reference sphere was measured in pixels, allowing us to calculate a conversion factor ( $r_s = \text{diameter}^2 \text{ diameter}^{-2}$ ; mm<sup>2</sup> pixel<sup>-1</sup>) between image pixels and physical dimensions. All non-shoot imagery (purple background, black tape, extra length of twig, and reference sphere) was removed from each photograph in Photoshop (Adobe Photoshop CS, Adobe System).

Shoot silhouette area in the shoot photographs and  $A_{PN}$  in the needle photographs were obtained as the sum of the non-zero pixels in each photograph. Shoot envelope area equaled the area of the resulting polygon. These calculations were performed in Matlab (Matlab Release 14, MathWorks, Natick, MA).

Until the accuracy of modeled total needle surface area ( $A_N$ ) was verified in the investigation on the three intensively studied pine species,  $A_N$  was calculated from  $A_{PN}$  measured from photographs. When estimating  $A_{PN}$  from photographs, we assumed that, for the pine species, needles placed on a horizontal surface have no preferred orientation, resulting in  $A_{PN}$  being a measure of the cylindrical mean of the projected needle area. Further, assuming the needles have concave cross-sections, we obtained  $A_N/A_{PN} = \pi$  for the pine species.

#### Model-based approach

**Algorithm and software** We constructed the computational shoot model using the mathematical framework of L-systems. L-Systems were first designed to simulate growth of simple multicellular organisms (Lindenmayer 1968). Integration of geometric features into models using L-systems enables the use of computer graphics for realistic visualization of plant structures (Prusinkiewicz and Lindenmayer 1990). The syntax and grammar used in this study have been described by Prusinkiewicz and Lindenmayer (1990) and were originally coded by Lapré (<http://home.wanadoo.nl/laurens.lapre/>). With needle and twig dimensions as inputs, the model generates a 3D representation of the shoot. The simulated object can then

be analyzed with standard image processing tools to provide estimates of shoot silhouette and envelope areas.

Our L-systems model was designed to account for 12 measured inputs: twig length, twig diameter, twig apex and base  $\theta$ , number of fascicles, needle width, needle length and attachment angle at twig apex and base, and lateral and vertical asymmetries. In addition, needle deflection to length ratio was measured once for each species. These inputs were translated, by a Matlab code, into a set of growth rules following the L-systems syntax and fed to the L-systems program modified from Lapré's model. The program produced a 3D, highly detailed Virtual Reality Markup Language file (VRML1.0) that included a modeled reference sphere to scale the model shoot. The output file was opened in Amira (Amira 3.1.1, Mercury Computer System GmbH, Berlin, Germany) under orthographic view where a Tool Command Language (TCL) code mimicked our modified optical approach to manipulate the 3D rendered object. The modeled shoot positions were chosen to match the nineteen photographs taken from each shoot, and high-resolution ( $1280 \times 1000$  pixels) uncompressed screenshots were saved. The screenshots were then processed in Matlab based on the same method described for the photographs. The stochastic components in the model (needle length and angle) allowed reproduction of the measured distributions of the geometric characteristics that were used as inputs for the model.

Lapré's model can be used to simulate a wide range of growth patterns based on simple length and angle measurements of a shoot. However, the software lacked several features that were essential to capturing shoot structure: as originally implemented, gravity produced spirally bending needles; simulation of randomly distributed parameters was possible only for angles and only through a uniform random number generator; and changes in length according to the L-systems syntax led to width changing accordingly. To generate better control of the physical behavior of the generated shoots, we modified the model as follows. (1) We replaced the gravity model with one based on beam deflection. Each needle segment deviated slightly from the previous segment along a vertical plane using a rotation angle. The new model ensured that positive gravity was always simulated as a downward, vertical vector. Negative gravity values were used to simulate the growth of twigs toward the light. (2) We changed the uniform random number generator with a Gaussian one. We adapted the random routine to allow for normal variability in needle length around mean values. (3) We created extra variables to record length and width variations separately, to simulate elements of different lengths with the same diameter.

**Model structure and parameterization** In our model, the twig was described as a cylinder with needles that were either individually positioned with or without petioles, or grouped in fascicles of two or more. The attachment points of needles or fascicles could be either cylindrically distributed around the twig according to a spiral pattern, or positioned on both sides of the twig for planar shoots. In addition, to account for the effects of growth constraint on the display of needles attached to the

shoot, two asymmetry parameters were used in the shoot model. The lateral asymmetry parameter described the location of needles relative to a vertical plane through the shoot axis. The vertical asymmetry parameter was used to model inclined shoots with a strong difference in needle distribution above and below the twig. The lateral asymmetry parameter was set to +1 or -1 if more than 2/3 of the needles were on the right hand or left hand side of the shoot from base to apex, respectively, and 0 otherwise. Similarly, the vertical asymmetry parameter was set to +1 or -1 if more than 2/3 of the needles were above or below the shoot from base to apex, respectively, and 0 otherwise. Because of the cylindrical symmetry of the spherical integration, the sign of the lateral asymmetry parameter had no effect on the RTM parameters estimated with the model. In our model, the elasticity modulus was not calculated but its effects were simulated through the gravity routine of the model. We defined a species-specific bending parameter as the mean deflection to needle length ratio. This resulted in realistic bending of needles and twigs.

Shoots were modeled by relating twig and needle dimensions (twig length, diameter and absolute inclination angle, and needle length, width and angle) to the position along the twig. In our three intensively studied species, the needles were grouped in fascicles of two (*P. echinata*) or three (*P. taeda* and *P. palustris*), and the fascicles were organized spirally along the shoot. Our observations showed that needle length and needle angle varied linearly from the base to the apex of the shoot (data not shown). Specifically, plots of relative length versus relative position on the twig showed that needle length: (1) decreased linearly with distance from the base of *P. echinata* shoots ( $r^2 = 0.45$ ); (2) was highly variable around a mean value for shade shoots of *P. taeda*; and (3) increased to a plateau for *P. palustris* and sun shoots of *P. taeda* ( $r^2 = 0.78$  and  $0.59$ , respectively). For the latter shoot types though, use of a linear approximation led to < 1.5% underestimation of  $A_N$  and SSA.

Relative needle angle was poorly related to relative position in all species. It decreased linearly with distance from the base ( $r^2$  ranging from 0.15 for *P. taeda* shade shoots to 0.36 for *P. palustris*), except in the sun shoots of *P. taeda* in which the angle was highly variable around a mean value ( $r^2 = 7 \times 10^{-5}$ ). Thus, needle angle on the shoot was modeled as a linear interpolation between the means of values measured at the base and apex of the shoots. These mean values were calculated from eight fascicles at each location.

We modeled  $A_N$  from means of needle length and width, and needle cross section (perimeter). Needle width was unrelated to position along the twig, and thus, the mean value measured in each shoot was used in the model. We did not aim to reproduce the actual cross-sectional shape of needles, which would increase the number of polygons and computational time. Instead, we modeled the cross sections as triangles such that modeled needles and actual needles had similar cross-sectional perimeters. Thus, we approximated needle cross sections as triangles with opening angles of  $164^\circ$  for *T. canadensis* (flat needles),  $82^\circ$  for *P. taeda* and *P. palustris*,  $75^\circ$  for

*P. echinata* and *P. thumbergiana* and 60° for *P. strobus* and *P. pungens*. We modeled the tips of needles as triangles to simulate the taper observed on sampled shoots. We also made the needles more realistic by adding a 9° twisting rotation from one needle segment to the next except for *P. pungens* (no observed rotation) and *T. canadensis* (4.5°). This twist was mostly cosmetic and did not modify the simulated  $\overline{STAR}$  and  $c$ . Finally,  $A_T$  was calculated assuming a cylindrical shape for the twig.

#### Statistical analyses

Least-square linear regressions, one-way ANOVA and *t*-tests were performed in SAS (SAS Institute, Cary, NC). The differences between linear regressions were tested by the extra sum of squares principle (Ramsey and Schäfer 1997).

## Results

#### Comparison between the standard and the proposed optical method

We compared our approach to the standard photographic method recently used for *Pinus taeda* and *P. palustris* (Niinemets et al. 2006). For each species, a shoot was first processed by our approach (Figure 1) and then by the standard approach, i.e., changing both the shoot orientation and inclination angles in front of a camera maintained at a fixed position. For the relatively stiff shoots of *P. echinata*,  $STAR(\phi, \theta)$  and  $c(\phi, \theta)$  obtained with the two methods were similar at all view angles. When processing larger, more flexible shoots (*P. taeda* and *P. palustris*), the needles and twig bent differently relative to the camera position, particularly at low  $\theta$ . Values of  $STAR(\phi, \theta)$  and  $c(\phi, \theta)$  obtained with the two methods differed accordingly.

Cylindrical means of  $STAR$  and  $c$  (Equation 3 and  $c_{cyl}(\theta)$  defined likewise) were computed from the six rotation angles at all  $\theta$  for each shoot (expressed in Figure 2 as the difference between fixed and moving camera values normalized by the moving camera values).

$$STAR_{cyl}(\theta) = \int_{-\pi}^{\pi} STAR(\phi, \theta) d\phi \quad (3)$$

The apparent similarity observed at all angles for the stiff shoot of *P. echinata* led to similar  $STAR_{cyl}$  and  $c_{cyl}$  ( $n = 6$ ; minimum  $P = 0.2$ ). However, the bending imposed on flexible shoots of the other two pines by the standard method caused underestimation of the cylindrical mean by up to ~30% ( $P = 0.001$ ) for  $STAR_{cyl}$  and ~20% (single measurement at  $\theta = 0^\circ$ ) for  $c_{cyl}$ . Spherical means of the parameters were weighted toward larger  $\theta$ . For *P. palustris*, the species with the most flexible shoots, the standard method resulted in a 10% ( $P = 0.002$ ) underestimation of  $STAR$ , but the canceling errors in the spherically averaged shoot silhouette areas ( $SSA$ ; -10%;  $P = 0.002$ ) and envelope areas ( $SEA$ ; -13%;  $P < 0.001$ ) resulted in only a small effect on the estimate of  $c$  (2%;  $P = 0.03$ ).

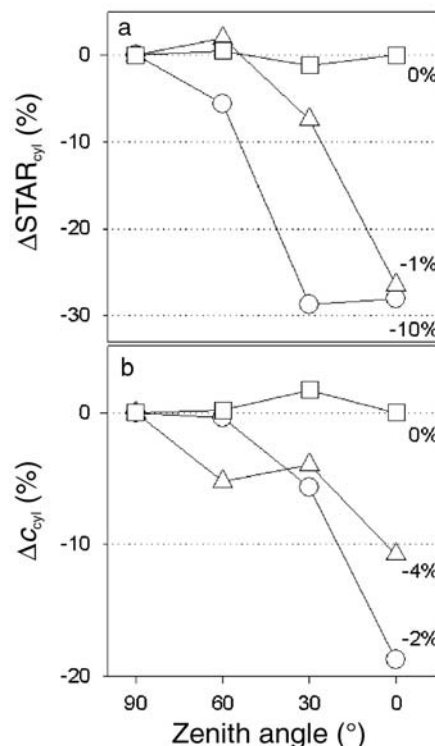


Figure 2. Relative difference between values from the standard, fixed-camera, photographic method and the values from the mobile camera approach. (a) Cylindrically averaged shoot silhouette-to-leaf area ratio ( $STAR_{cyl}$ ). (b) Cylindrically averaged transmission coefficient ( $c_{cyl}$ ). Differences between the spherically weighted means are indicated for each species. Symbols: ○ = *Pinus palustris*; △ = *P. taeda*; and □ = *P. echinata*.

#### Model validation

For the three intensively studied species (*P. echinata*, *P. taeda* and *P. palustris*), the screenshots of the virtual shoots appeared similar to photographs of these shoots when compared at similar view angles (Figure 3). Our photography-based and modeled  $SSA(\phi, \theta)$  and  $SEA(\phi, \theta)$  matched well at all angles (not shown). Consequently the estimates of  $SSA$  and  $SEA$  were similar (Figures 4a and 4b). Total needle surface area, calculated from  $A_{PN}$  obtained by the photographic method, was also computer-generated based on needle dimensions. The simulated needles projected on a horizontal surface without overlap led to an estimate of  $A_N$  similar to that from the photographs of needles similarly placed on a flat surface (Figure 4c). In general, there were no statistically significant differences between the photography-based and modeled values of  $SSA$ ,  $SEA$  and  $A_N$  for any of the species or canopy position (paired *t*-tests with minimum  $P = 0.14$ ). Moreover, the general relationships between modeled and optically measured quantities did not differ from the 1:1 line for any of the three variables ( $P > 0.05$ ).

Because the model was able to reproduce the estimates of  $SSA$ ,  $SEA$  and  $A_N$  based on photography, the modeled and photography-based estimates of  $STAR$  and  $c$  were also similar (Figures 5a and 5b). The sample mean of  $STAR$  and  $c$  of sun shoots of *P. echinata*, *P. taeda* and *P. palustris* were similar and

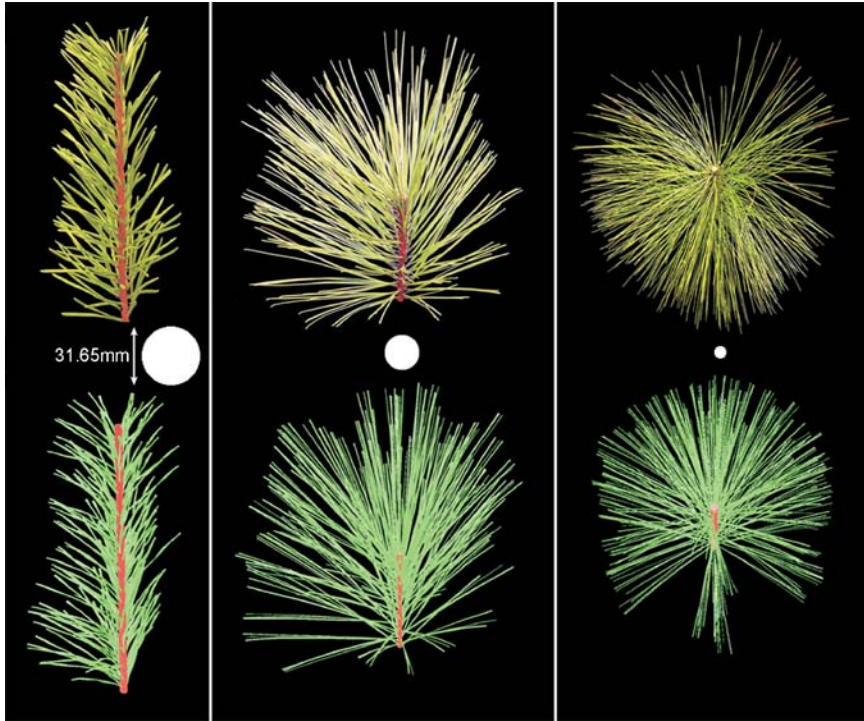


Figure 3. Comparison between actual shoots (upper row) and their corresponding models for (left to right) *Pinus echinata*, *P. taeda* and *P. palustris* (all reference disks have the same diameter).

significantly lower than  $\overline{STAR}$  and  $c$  of shade shoots of *P. taeda* (Table 2). Within each species, the values of  $\overline{STAR}$  and  $c$  were positively correlated, and at a given  $c$ ,  $\overline{STAR}$  was higher in species with short needles than in species with long needles (Figure 5c).

Within each species,  $\overline{SSA}$  was strongly correlated with  $A_N$  (Figure 6). Figure 6a shows all data from this study and also includes additional data for *Pinus sylvestris* L. (Stenberg et al. 2001) and *Picea abies* (L.) Karst. (Palmroth et al. 2002). For small shoots (Figure 6b), unfertilized *P. abies* generated less  $\overline{SSA}$  for a given  $A_N$  than *P. sylvestris* and fertilized *P. abies*. The *P. sylvestris* and fertilized *P. abies* shoots, in turn, shared the same relationship with the larger shoots of the three southern pine species (Figure 6c). Differences among regression lines were determined based on  $P = 0.05$ . Each of the relationships had a small positive intercept ( $P < 0.05$ ) because the projected twig area is included in  $\overline{SSA}$  but not in  $A_N$ . Despite the statistical differences shown in Figures 6a and 6b, the absolute differences were small. Combining the entire dataset (Figure 6a) led to an overall relationship of  $\overline{SSA} = 0.16A_N$

( $r^2 = 0.982$  or  $\overline{SSA} = 0.159A_N^{0.985}$ ,  $r^2 = 0.980$ ), suggesting that  $\overline{STAR}$ , uncorrected for twig area, was roughly constant.

To evaluate the ability of the model to generate shoots with different architectural characteristics, single shoots of additional pine and other coniferous species were processed. *Pinus strobus* was chosen for its flexible needles, *P. thunbergiana* for its long yet stiff needles, *Picea pungens* for its organized structure and *Tsuga canadensis* for the near random organization of its needles in a plane. In addition, we generated two current-year shoots of *P. palustris* in which needles were more clumped than in 1-year-old shoots. The shoots were visually well reproduced by the model when compared with photographs (Figure 7). Moreover, both spherical (Figure 8) and cylindrical (Figure 9) means of  $\overline{STAR}$  and  $c$  retrieved from the photographs were similar to the modeled estimates.

**Discussion**

We developed an architectural model for a coniferous shoot with bending needles and shoots and modified an existing pho-

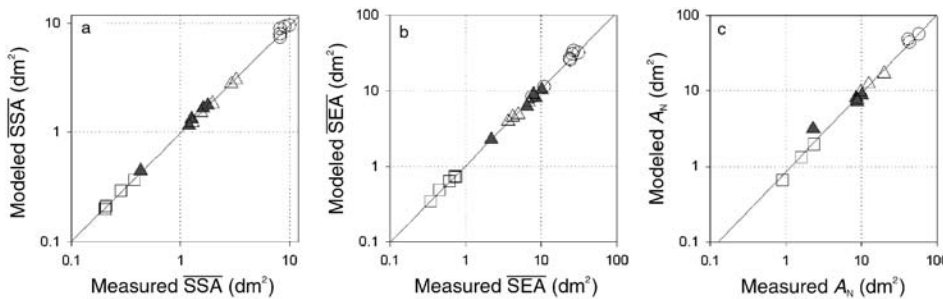


Figure 4. Comparison of estimates of (a) spherically averaged shoot silhouette area (SSA), (b) spherically averaged shoot envelope area (SEA) and (c) total needle area ( $A_N$ ) measured from photographs and estimated based on the model. Symbols:  $\circ = Pinus palustris$ ;  $\triangle = P. taeda$ ;  $\square = P. echinata$ ; and  $\blacktriangle = P. taeda$  shoots from the bottom of the canopy.

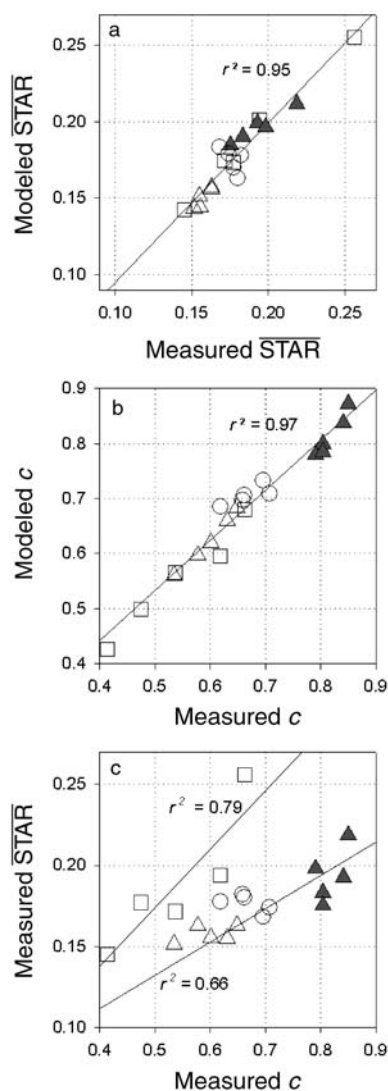


Figure 5. Comparison of modeled and photographically measured (a) spherically averaged silhouette to leaf area ratio (STAR) and (b) transmission coefficient ( $c$ ). Symbols:  $\circ$  = *Pinus palustris*;  $\triangle$  = *P. taeda*;  $\square$  = *P. echinata*; and  $\blacktriangle$  = *P. taeda* shoots from the bottom of the canopy.

topography-based method to produce test data for the model. The model produced reliable estimates of silhouette and envelope areas at various view angles for species with shoots that range in size and structure. The model was designed to enable spherical and cylindrical averaging of important structural parameters and to separate the effect of shoot orientation from that of shoot structure on potential light interception and transmission.

Both  $\overline{\text{STAR}}$  and  $c$  were similar in the sun-acclimated shoots of the three pine species studied despite large apparent differences in the structure of their shoots (Table 2). Similar to previous investigations on other conifers (Sprugel et al. 1996, Stenberg et al. 1999, 2001, Cescatti and Zorer 2003, Niinemets et al. 2006), our  $\overline{\text{STAR}}$  value for shade shoots of *Pinus taeda* was higher than for sun shoots. This increase in  $\overline{\text{STAR}}$  with

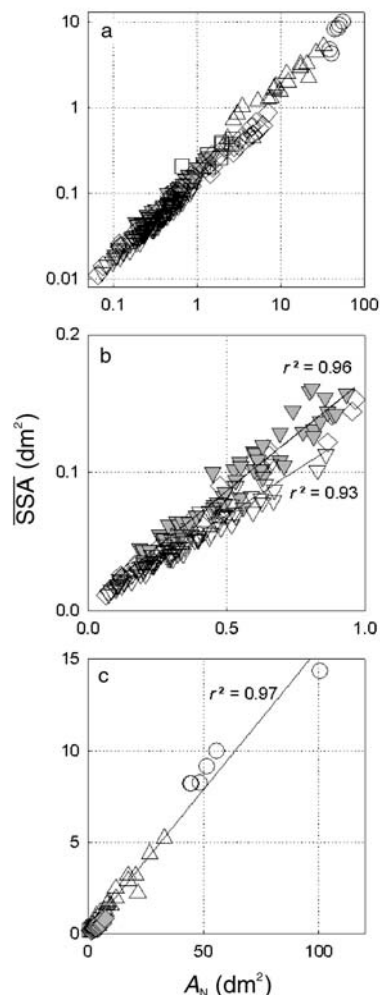


Figure 6. Spherically averaged shoot silhouette area ( $\overline{\text{SSA}}$ ) as a function of total needle area ( $A_N$ ) (a) for the combined data on a log-log scale, (b) for small shoots and (c) for large shoots. Symbols:  $\circ$  = *Pinus palustris*;  $\triangle$  = *Pinus taeda*;  $\square$  = *Pinus echinata*;  $\blacktriangledown$  = *Picea abies* in irrigated fertilized plots;  $\nabla$  = control *Picea abies*; and  $\diamond$  = *Pinus sylvestris*.

shading of *P. taeda* shoots was accompanied by an increase in  $c$ , yet the relationship between the two parameters was not generalizable, indicating that certain attributes of shoot structure affected one parameter differently from the other (Figure 5c). Among all the sun-acclimated shoots investigated,  $c$  increased with increasing flexibility of needles (Figure 8b), which was largely correlated with needle length. However, the observed variation in  $\overline{\text{STAR}}$  was unrelated to shoot or needle size (Figure 8a).

Certain shoot characteristics, e.g., needle area per unit of twig length, have been shown to explain a large part of the variation in  $\overline{\text{STAR}}$  in some species (Stenberg et al. 2001). These shoot characteristics can be used to estimate  $\overline{\text{STAR}}$  values in canopy RTM of such species. We showed that a fairly strong relationship emerged between  $\overline{\text{SSA}}$  and  $A_N$  (Figure 6). In both small and large shoots (indicated by the two ranges in  $A_N$  in Figure 6b versus 6c), those with lower needle density had

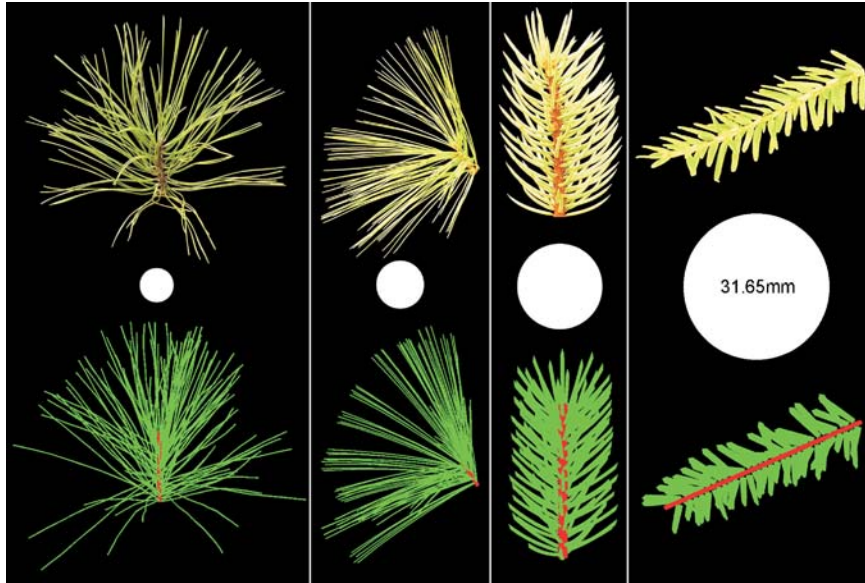


Figure 7. Photographed shoots (top) and their corresponding modeled shoots (bottom) for (left to right) *Pinus thumbergiana*, *Pinus strobus*, *Picea pungens* and *Tsuga canadensis* (all reference disks have the same diameter).

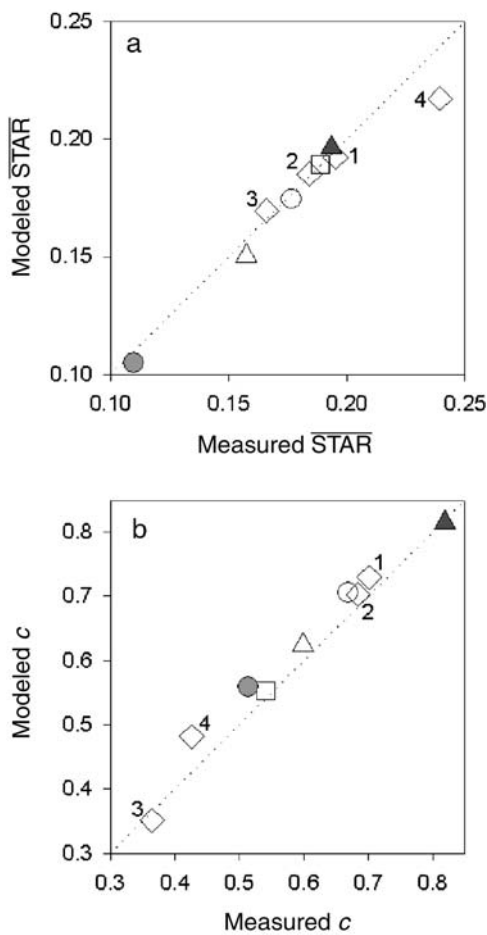


Figure 8. Comparison of modeled and photographically measured (a) spherically averaged silhouette-to-total leaf area ratio (STAR) and (b) transmission coefficient ( $c$ ) for one shoot of *Pinus thumbergiana* (1), *Pinus strobus* (2), *Picea pungens* (3) and *Tsuga canadensis* (4), the mean of two current-year shoots of *Pinus palustris* (●) and the means of species and positions shown in Figures 5a and 5b.

higher  $\overline{SSA}$  at a given  $A_N$ . In particular, small shoots of fertilized *Picea abies* had higher  $\overline{SSA}$  than unfertilized *P. abies*. Although species and growing conditions affected the relationship between  $\overline{SSA}$  and  $A_N$ , the overall relationship between these variables provides a first, rough approximation of STAR ( $\sim 0.16$ ) for species for which there are no data.

A better approach to estimate STAR and  $c$  is to rely on architectural models. In combination with computer graphics techniques such as ray-tracing methods (Ross and Marshak 1988), architectural models provide a powerful tool for studying the interactions between canopy architecture and the radiation regime. One such architectural model was developed by Oker-Blom et al. (1983) for *Pinus sylvestris* shoots and has been used in studies of shoot penumbral radiation (Stenberg et al. 1995, Palmroth et al. 1999). The model has also been used to study the effects of shade acclimation on shoot-level light interception and photosynthesis (Stenberg et al. 2001), and the effects of multiple scattering within shoots on canopy reflectance (Smolander and Stenberg 2003, 2005). Our model differed from that of Oker-Blom et al. (1983) in that it was designed to handle bending structures. This allowed processing of large shoots with long needles, such as those of many pine species. Furthermore, interfacing the architectural model with 3D visualization software added a new dimension to the model validation process by allowing visual inspection of the shoot representation.

Most importantly, unlike other methods, our model offered great flexibility in the simulation of STAR and  $c$ . For example, silhouette-to-leaf area ratio could be defined in a number of ways. Originally, only the maximum value of STAR ( $STAR_{max}$ ) was estimated (Table 1). Later, STAR was introduced, not correcting for the contribution of the twig to the silhouette area. Recently, the effect of twig area on STAR was accounted for by adding it to  $A_N$  (Stenberg et al. 1999). Our model permitted both the estimation of these three representations and an additional one by removing the twig from the sil-

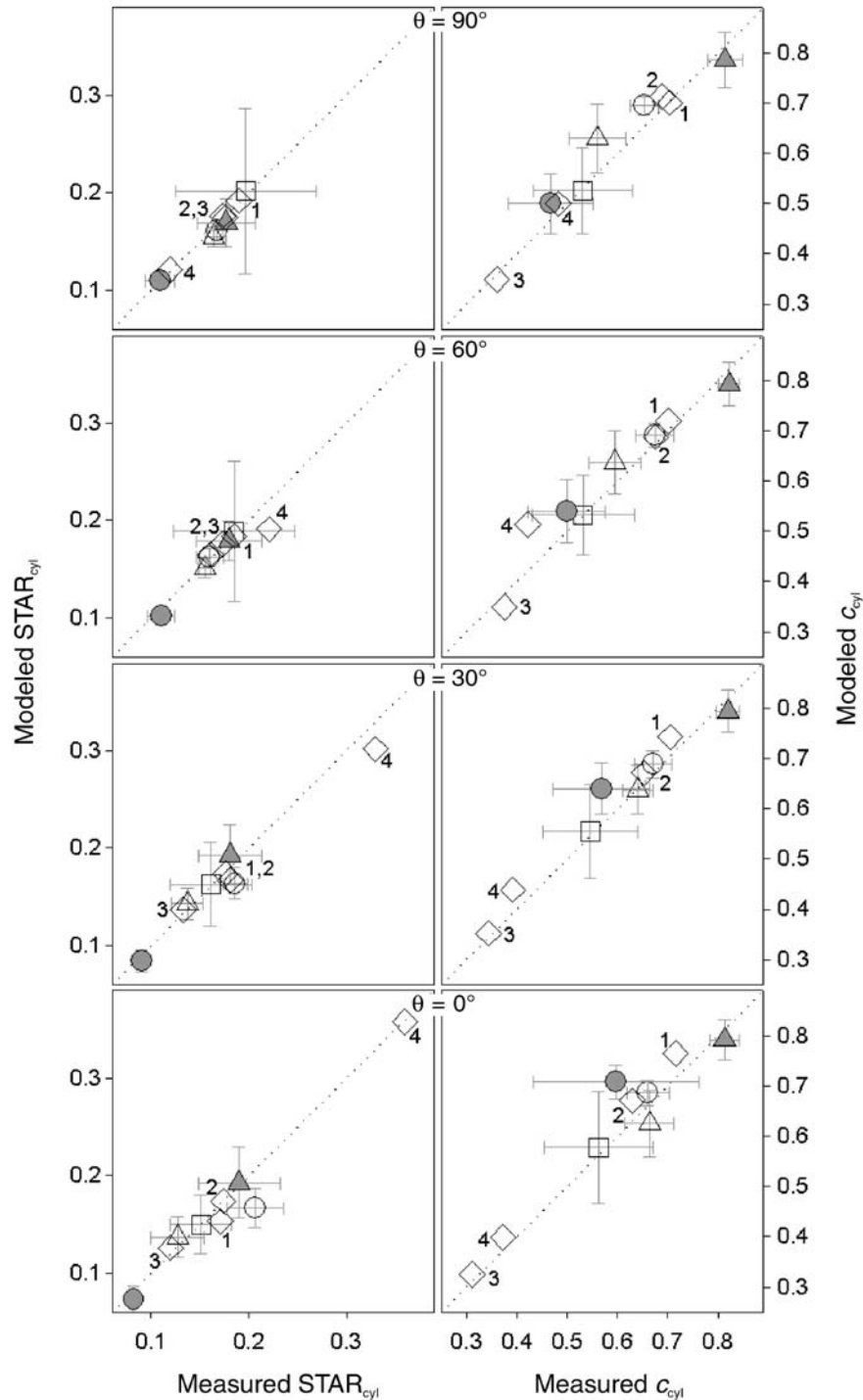


Figure 9. Comparison of modeled and photographically measured cylindrically averaged silhouette-to-total leaf area ratio ( $STAR_{cyl}$ ) (left panels) and transmission coefficient ( $c_{cyl}$ ) (right panels) of all studied species for all zenith angles ( $\theta$  ranging from  $90^\circ$  to  $0^\circ$  in  $30^\circ$  intervals from top to bottom panels). Symbols:  $\diamond$  = *Pinus thumbergiana* (1), *Pinus strobus* (2), *Picea pungens* (3) and *Tsuga canadensis* (4);  $\square$  = *Pinus echinata*;  $\triangle$  and  $\blacktriangle$  = sun and shade shoots of *Pinus taeda*, respectively; and  $\circ$  and  $\bullet$  = previous-year and current-year shoots of *Pinus palustris*, respectively.

houette area of the generated shoot (Table 1). Obtaining this new calculation of STAR through photography is time consuming and difficult to do with reasonable accuracy, whereas generating it with our model required no additional computational time. Furthermore, the flexibility of the model extended to accurate estimation of cylindrical means of STAR and  $c$  for a wide range of species (Figure 9), allowing its use for applications where zenith-specific estimates of those parameters are needed (e.g., Möttus 2004). All variants of shoot parameters

were generated in a single model run, and processing each shoot, including measuring the requisite attributes necessary as model inputs (Table 2) and computing the output parameters, took about 15 minutes.

The model can be used as a basic unit in canopy-level 3D models. Increasing the realism in the description of canopy structure by incorporating the 3D shoots leads to complex RTMs that are impractical and unnecessary in many applications. Explicit 3D RTMs, however, are essential for assessing

the impact of simplifications in more aggregated models. Validating canopy photosynthesis models is difficult because neither PAR on leaf surfaces nor canopy photosynthesis can be measured directly. However, if the structure and distribution of the canopy elements are described sufficiently well, calculations of the radiation budget and thus estimates of photosynthesis are more accurate. Complex models can provide benchmark estimates for guiding the development of simpler aggregated models.

The architectural model presented here can be improved further. Local variations in incoming light and physical interaction with other shoots lead to irregularities in the shoot architecture that are difficult to quantify. Currently, we separate asymmetry into left-right and up-down flags that should be easily discerned by even an untrained investigator. However, a more refined classification would make the 3D representation of the shoot more realistic, further improving STAR and  $c$  estimates. Second, a primary motivation for developing the shoot model was to describe the bending of needles and shoots. Gravity is currently simulated as a rotation from one segment to the next depending on the local orientation and on a measure of needle deflection to needle length ratio (referred to as bending parameter). This approximation led to deflections visually close to predictions based on solid mechanics equations. The bending parameter was evaluated for each species and mimics Young's elasticity modulus (stiffness  $E$ , or rate of change of stress with strain). A more mechanistically accurate description would require a more detailed physical description of needles. This, together with honing the asymmetry routine, should streamline the model application across species. It might also reduce the number of input variables required and simplify the model interface.

#### Acknowledgments

This research was supported by the Office of Science (BER), U.S. Department of Energy, Grant No. DE-FG02-95ER62083 and the Academy of Finland Grant No. 52228. We thank Pekka Voipio and Yavor Parashkevov for help in the development of the measuring system.

#### References

- Anderson, M.C. 1971. Radiation and crop structure. *In* Plant Photosynthetic Production. Eds. Z. Šesták, J. Čatský and P.G. Jarvis. Dr. W. Junk, The Hague, pp 412–466.
- Carter, G.A. and W.K. Smith. 1985. Influence of shoot structure on light interception and photosynthesis in conifers. *Plant Physiol.* 79:1038–1043.
- Cescatti, A. and R. Zorer. 2003. Structural acclimation and radiative regime of silver fir (*Abies alba* Mill.) shoots along a light gradient. *Plant Cell Environ.* 26:449–442.
- Chen, J., P.M. Rich, S.T. Gower, J.M. Norman and S. Plummer. 1997. Leaf area index of boreal forests: theory, techniques and measurements. *J. Geophys. Res.* 102(D24):29,429–29,443.
- Knyazikhin, Y., J.V. Martonchik, R.B. Myneni, D. Diner and S.W. Running. 1998. Synergistic algorithm for estimating vegetation canopy leaf area index and fraction of absorbed photosynthetically active radiation from MODIS and MISR data. *J. Geophys. Res.* D103:32,257–32,276.
- Leverenz, J.W. and T.M. Hinckley. 1990. Shoot structure, leaf area index and productivity of evergreen conifer stands. *Tree Physiol.* 6:135–149.
- Lindenmayer, A. 1968. Mathematical models for cellular interaction in development. Parts I and II. *J. Theor. Biol.* 18:280–315.
- McCarthy, H.R., R. Oren, A.C. Finzi, D.S. Ellsworth, H.-S. Kim, K.H. Johnsen and B. Millar. 2007. Temporal dynamics and spatial variability in the enhancement of canopy leaf area under elevated atmospheric CO<sub>2</sub>. *Glob. Change Biol.* In press.
- Miller, E.E. and J.M. Norman. 1971. A sunfleck theory for plant canopies. I. Lengths of sunlit segments along a transect. *Agron. J.* 63:735–738.
- Miller, P.C. 1967. Leaf temperature, leaf orientation, and energy exchange in quaking aspen (*Populus tremuloides*) and Gambell's oak (*Quercus gambellii*) in central Colorado. *Oecol. Plant.* 2:241–270.
- Möttus, M. 2004. Measurement and modeling of the vertical distribution of sunflecks, penumbra and umbra in willow coppice. *Agric. For. Meteorol.* 121:79–91.
- Niinemets, U., M. Tobias, A. Cescatti and A. Sparrow. 2006. Size dependant variation in shoot light-harvesting efficiency in shade-intolerant species. *Int. J. Plant Sci.* 167:19–32.
- Nilson, T. 1971. A theoretical analysis of the frequency of gaps in plant stands. *Agric. Meteorol.* 8:25–38.
- Nilson, T. and J. Ross. 1997. Modeling radiative transfer through forest canopies: implications for canopy photosynthesis and remote sensing. *In* The Use of Remote Sensing in the Modeling of Forest Productivity. Eds. H.L. Gholz, K. Nakane and H. Shimoda. Kluwer Academic Publishing, Dordrecht, pp 23–60.
- Norman, J.M. and P.G. Jarvis. 1975. Photosynthesis in Sitka spruce (*Picea sitchensis* (Bong.) Carr.)—radiation penetration theory and a test case. *J. Appl. Ecol.* 12:839–878.
- Oker-Blom, P. and H. Smolander. 1988. The ratio of shoot silhouette area to total needle area in Scots pine. *For. Sci.* 34:894–906.
- Oker-Blom, P., P. Kellomäki and H. Smolander. 1983. Photosynthesis of a Scots pine shoot: the effect of shoot inclination on the photosynthetic response of a shoot subjected to direct radiation. *Agric. Meteorol.* 29:191–206.
- Oker-Blom, P., M.R. Kaufmann and M.G. Ryan. 1991. Performance of a canopy light interception model for conifer shoots, trees and stands. *Tree Physiol.* 9:227–243.
- Palmroth, S., L. Palva, P. Stenberg and A. Kotisaari. 1999. Fine scale measurement and simulation of penumbral radiation formed by a pine shoot. *Agric. For. Meteorol.* 95:15–25.
- Palmroth, S., P. Stenberg, S. Smolander, P. Voipio and H. Smolander. 2002. Fertilization has little effect on light interception efficiency of *Picea abies* shoots. *Tree Physiol.* 22:1185–1192.
- Prusinkiewicz, P. and A. Lindenmayer. 1990. The algorithmic beauty of plants. Springer-Verlag, New York, 240 p. Available online at <http://algorithmicbotany.org/papers/abop/abop.pdf>.
- Ramsey, F.L. and D.W. Schäfer. 1997. The statistical sleuth: a course in methods of data analysis. Duxbury Press, Belmont, CA, 742 p.
- Ross, J. 1981. The radiation regime and architecture of plant stands. Dr. W. Junk, The Hague, 391 p.
- Ross, J.K. and A.L. Marshak. 1988. Calculation of canopy bidirectional reflectance using the Monte Carlo method. *Remote Sens. Environ.* 24:213–225.
- Ryel, R.J., E. Falge, U. Joss, R. Geyer and J.D. Tenhunen. 2001. Penumbral and foliage distribution effects on *Pinus sylvestris* canopy gas exchange. *Theor. Appl. Clim.* 68:109–124.
- Schäfer K., R. Oren, D.S. Ellsworth, C.T. Lai, J.D. Herrick, A.C. Finzi, D.D. Richter and G.G. Katul. 2003. Exposure to an enriched CO<sub>2</sub> atmosphere alters carbon assimilation and allocation in a pine forest ecosystem. *Glob. Change Biol.* 9:1378–1400.

- Shabanov, N.V., Y. Knyazikhin, F. Baret and R.B. Myneni. 2000. Stochastic modeling of radiation regime in discontinuous vegetation canopies. *Remote Sens. Environ.* 74:125–144.
- Smolander, S. and P. Stenberg. 2003. A method to account for shoot scale clumping in coniferous canopy reflectance models. *Remote Sens. Environ.* 88:363–373.
- Smolander, S. and P. Stenberg. 2005. Simple parameterizations of the radiation budget of uniform broadleaved and coniferous canopies. *Remote Sens. Environ.* 94:355–363.
- Smolander, S., P. Stenberg and S. Linder. 1994. Dependence of light interception efficiency of Scots pine shoots on structural parameters. *Tree Physiol.* 14:971–980.
- Sprugel, D.G., J.R. Brooks and T.M. Hinckley. 1996. Effect of light on shoot and needle morphology in *Abies amabilis*. *Tree Physiol.* 16:91–98.
- Stenberg, P. 1996. Correcting LAI-2000 estimates for the clumping of needles in shoots of conifers. *Agric. For. Meteorol.* 79:1–8.
- Stenberg, P. 1998. Implication of shoot structure on the rate of photosynthesis at different level in a coniferous canopy using a model incorporating grouping and penumbra. *Funct. Ecol.* 12:82–91.
- Stenberg, P., S. Linder, H. Smolander and J. Flower-Ellis. 1994. Performance of the LAI-2000 plant canopy analyzer in estimating leaf area index of some Scots pine stands. *Tree Physiol.* 14:981–995.
- Stenberg, P., S. Linder and H. Smolander. 1995. Variation in the ratio of shoot silhouette area to needle area in fertilized and nonfertilized Norway spruce trees. *Tree Physiol.* 15:705–712.
- Stenberg, P., H. Smolander, D. Sprugel and S. Smolander. 1998. Shoot structure, light interception, and distribution of nitrogen in an *Abies amabilis* canopy. *Tree Physiol.* 18:759–767.
- Stenberg, P., T. Kangas, H. Smolander and S. Linder. 1999. Shoot structure, canopy openness, and light interception in Norway spruce. *Plant Cell Environ.* 22:1133–1142.
- Stenberg, P., S. Palmroth, B.J. Bond, D.G. Sprugel and H. Smolander. 2001. Shoot structure and photosynthetic efficiency along the light gradient in a Scots pine canopy. *Tree Physiol.* 21:805:814.
- Wang, Y.P., P.G. Jarvis and C.M.A. Taylor. 1991. PAR absorption and its relation to above-ground dry matter production of sitka spruce. *J. Appl. Ecol.* 28:547–560.